ORIGINAL ARTICLE

On the go-and-stop motion of the discontinuous precipitation front

M. Chronowski[1] · P. Zięba[2]

Abstract
The growth of lamellar structure during discontinuous precipitation occurs frequently by so-called go-and-stop fashion. The results of simulation combined with the changes of Cahn's parameter C revealed two types of such motion. The process takes place in the successive stages which can be distinguished judging from the value of C parameter. For lower values of linear growth rate ($v = 10 \div 20$ nm/s) and smaller α lamella thickness ($100 \div 200$ nm), the full cycle with relaxation takes 4–6 s. The faster movement of the reaction front ($v = 30$ nm/s) resulted in dramatic decrease of the full cycle to $\tau_{\text{total}} = 0.8$ s. The same behavior is observed if the α lamella thickness increases beyond 200 nm at constant v equal to 10 nm/s. Both predicted types of go-and-stop motion can experimentally be observed during growth or dissolution of discontinuous precipitates. What is the reason that particular type prevails is unknown, and this is invitation for further studies especially using high-resolution transmission electron microscope operating in in situ mode.

Keywords Discontinuous precipitation · Go-and-stop motion · Simulation of grain boundary diffusion · Cahn's parameter

1 Introduction

Discontinuous precipitation (DP) is the solid-state phase transformation during which the formation of the new phase occurs at the moving reaction front (RF) which is considered to be a high-angle grain boundary (GB). The transformation products represent usually the lamellar mixture of solute-rich new phase β and solute-depleted initial phase α having the same crystal structure as the starting supersaturated solid solution α_o.

In situ observation of the DP process in the high-voltage electron microscope [1] revealed that the movement of the α/α_o RF is not continuous but rather takes place in the go-and-stop fashion. The concept of the go-and-stop motion of the RF (called also jerky or oscillatory) was discussed in detail by Bögel and Gust [2]. They proposed the mechanism of periodical enrichment in the solute atoms at the RF or in its immediate vicinity. This event leads to a retardation and eventually to the stop of the RF migration. Then, the volume diffusion process becomes dominant, reducing the excess of solute atoms and the RF starts again to migrate.

In the case of diffusion-induced grain boundary migration (DIGM) [3] or discontinuous dissolution (DD) [4–10], the go-and-stop movement is frequently manifested by the presence of so-called "ghost images" (Fig. 1) existing in the regions swept by the migrating RF after etching with concentration-sensitive etchant. Here, the "ghost lines" parallel to the RF are likely to be associated with the stop stage, while the distance in between is relevant for the go stage.

Besides the "ghost lines," the "ghost traces" at the places where the β phase lamellae had previously existed were also revealed after DD process by means of optical microscopy [4, 5], scanning [6, 7] and transmission electron microscopy [8, 9]. They show strong enhancement of solute concentration as confirmed by an energy-dispersive X-ray microanalysis [9, 10].

One should note that in the case of DP reaction the "ghost lines" are not visible and the judgment about go-and-stop fashion of the RF motion results from the measurements of the growth distance versus time as in the in situ experiment of Abdou et al. [1]. Another possibility is to measure the solute concentration profiles across the α phase lamella at various distances behind the RF as in Refs. [11, 12].

✉ P. Zięba
p.zieba@imim.pl

1 AGH-University of Science and Technology, Kraków, Poland

2 Institute of Metallurgy and Materials Science, Polish Academy of Sciences, Reymonta St. 25, 30-059 Kraków, Poland
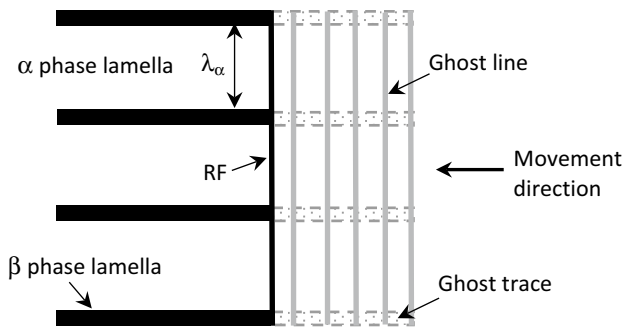
Fig. 1 Schematic representation of discontinuous dissolution with the formation of "ghost images"

In the present paper, the simple model valid for the DP process is presented which enables discrimination between go-and-stop periods based on the determination of dimensionless parameter C resulting from the solution of Cahn's equation [13].

2 Model

The model assumes that DP is a combined reaction of RF migration and RF diffusion [11]. It means that the solute atoms enter the α/α_o boundary by the diffusion along the RF toward the solute-rich β lamella. In order to achieve an equilibrium state within the α lamella, all the solute atoms have to diffuse along the boundary up to a distance of $\lambda_\alpha/2$ (λ_α—α lamella thickness) during displacement of the RF by its own width δ at the certain velocity v. Usually, the time allowed for the displacement is too short and some of the solute atoms do not arrive at the edge of the solute-rich β lamellae. They have to jump across the RF to enable the next elementary displacement. In this way, atoms which cross the RF contribute to form the solute concentration profile behind the RF. The number of atoms, which have to diffuse across the RF, increases with the further RF movement forming the solute profile. After a certain time, the number of atoms becomes so large that it may cause the stop of the RF to enable all the excessive atoms to enter the solute-depleted α lamella. Then, the RF gets relaxed and the process starts again.

In order to visualize such a process, the special procedure was prepared using HTML5, CSS3 and JavaScript technologies running on each device which supports website browsing (Fig. 2). The HTML was applied as a simple marker language in order to define positions of input data in user's browser, while CSS is a language used to describe styling: background colors, font sizes, input styles, etc. On the other hand, JavaScript was responsible for process animation, such as computing and redrawing the screen at given time interval. There are also two main canvases which are used to display the process and resulting parameters. Whole application is packed as one file, and it makes it easy to copy and run it on different devices.

The model is capable of simulating different cases using parameters which can be set by the user, such as:

v—linear growth rate of RF,
λ_α—α lamella thickness,
N_ε—amount of atoms entering the RF at time τ,
N_{max}—maximum amount of atoms entering the RF,
S—amount of sectors in the RF (from 0 to λ_α distance) used in the model,
C_p—capacity (maximum number of atoms) of each sector defined in the model.

One should emphasize that the simulation takes each sector into consideration and by using the least squares approximation is able to find function which has the best fit to the data. The simulation process can also be paused, continued and reset at any time. As the result, the solute concentration profiles left behind the moving forward RF of the discontinuous precipitates are obtained. They are described using Cahn's model [13] of DP reaction. The basic idea of this model is the balancing of the solute atom masses affected by diffusion along the RF and the motion of the RF. The solution takes the following form:

$$x(y) = (x_i - x_o)\,\frac{\cosh\left[(y - 0.5)\sqrt{C}\right]}{\cosh\left(\sqrt{C}/2\right)} + x_o \tag{1}$$
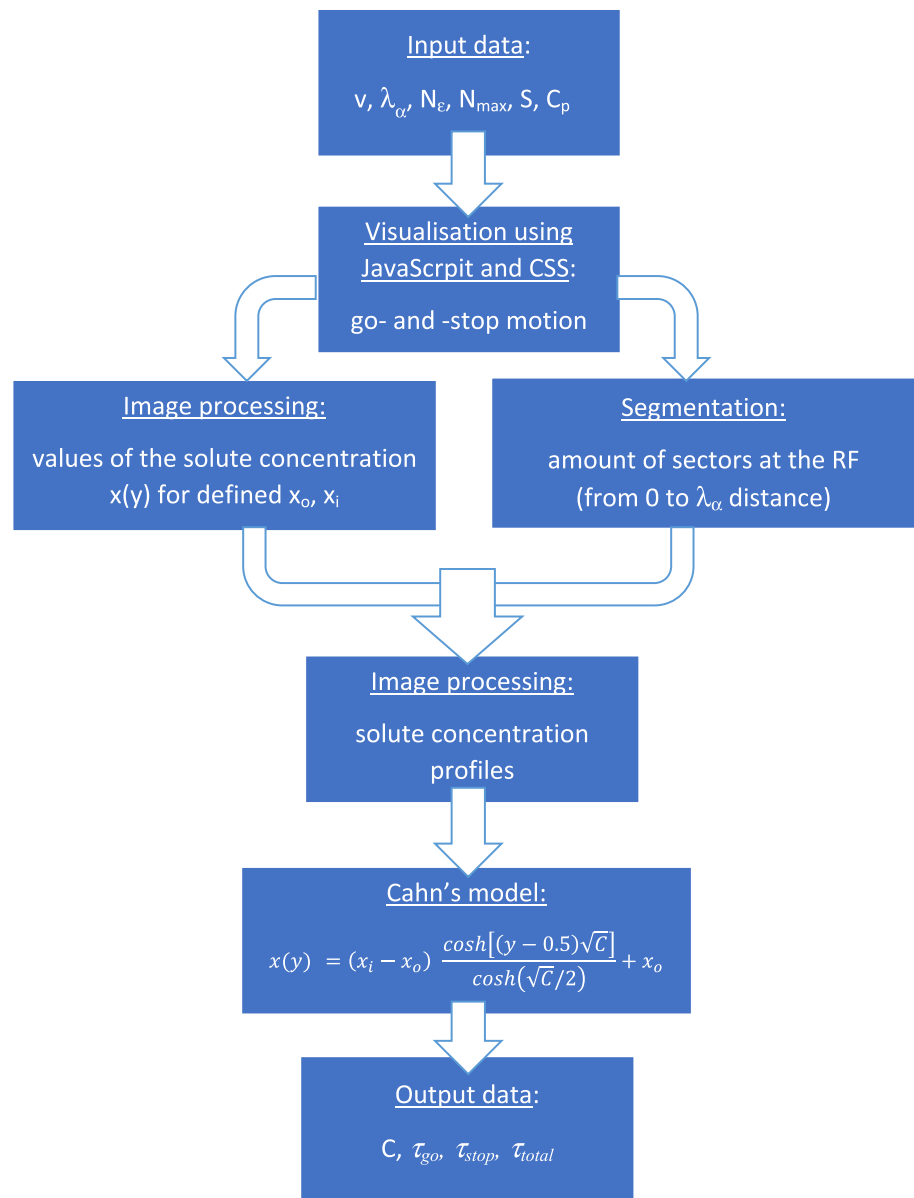
in which the parameter C is expressed by:

$$C = \frac{v\lambda_\alpha^2}{s\delta D_b} \tag{2}$$

Here, x_o is the original solute content in the alloy, x_i is the solute content in the α lamella in contact with the β lamella, v is the linear growth rate of RF, λ_α is the thickness of the α lamella, s is the segregation factor, δ is the grain boundary (RF) width, D_b is the grain boundary diffusion coefficient, and y is a co-ordinate measured from the edge of the β lamella in the direction perpendicular to the α lamella.

Except of C parameters, the simulation delivers, τ_{go}—time during which the RF moves, τ_{stop}—time necessary for all the RF excessive atoms to enter the solute-depleted α lamella (in other words time during which the RF is immobile) and τ_{total}—time of the whole process duration.

The simulation of the growth of discontinuous precipitates was performed at the example of Al-22 at.% alloy in which the DP process was described in detail including in situ observation [14, 15] and systematic studies

Fig. 2 Flowchart of simulation procedure

Input data:

v, λ_α, N_ε, N_{max}, S, C_p

Visualisation using JavaScrpit and CSS:

go- and -stop motion

Image processing:

values of the solute concentration $x(y)$ for defined x_o, x_i

Segmentation:

amount of sectors at the RF (from 0 to λ_α distance)

Image processing:

solute concentration profiles

Cahn's model:

$$x(y) = (x_i - x_o)\frac{cosh[(y - 0.5)\sqrt{C}]}{cosh(\sqrt{C}/2)} + x_o$$

Output data:

C, τ_{go}, τ_{stop}, τ_{total}

of the chemistry across the RF and α phase lamellae using analytical electron microscopy were performed [9, 16]. The input parameters for Eq. 1 were assumed to be $x_o = 22$ at.% and $x_i = 4.4$ at.%. Two cases were taken into consideration:

1. v = const, N_ε = const, for different values of λ_α,
2. λ_α = const, N_ε = const, for different values of v,

for which $v = 1 \times 10^{-8} \div 4 \times 10^{-8}$ m/s, $\lambda_\alpha = 1 \times 10^{-7} \div 4 \times 10^{-7}$ m. Those values are typical for the linear growth rate and α lamella thickness in Al-22 at.%

Zn alloy reported in the literature, see for example Refs. [9, 16].

3 Results

Figure 3 presents the schematic view of individual set of α and β phase lamellae. The solute concentration profiles formed during go (motion) period are visualized on the right side while those relevant for the stop (relaxation) period on the left side, and denoted as C_1, $C_2 \ldots C_9$, which corresponds to the values of Cahn's parameter expressed

Fig. 3 Schematic view of the growth of single cell during DP with accompanying solute concentration profile in go-and-stop period
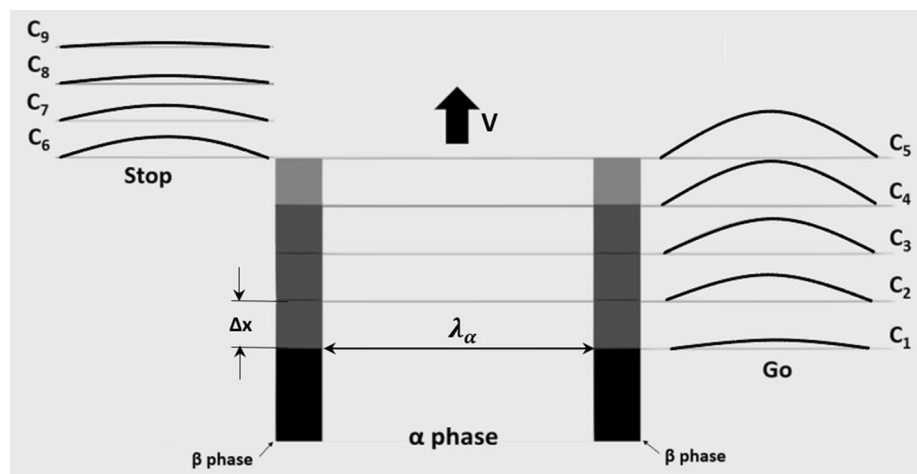
by Eq. 2. The distance of elementary movement of the reaction front was assumed to be equal to the RF width ($\delta = 5$ nm).

Table 1 contains details of the results obtained for the $\lambda_\alpha = 100$ nm and various values of the linear growth rate v. One can see that the C parameter increases up to maximum preceding the RF stopping and then decreases gradually up to $C = 0.89 \div 1.71$ which corresponds to hardly visible solute concentration profile. Time necessary for the go period (τ_{go}) and stop period (τ_{stop}) is 3 s for the initial $v = 10$ nm/s (Tables 1 and 2). The increase of linear growth rate v from 25 to 30 nm/s results in a dramatic decrease of τ_{go} and τ_{stop} to tenth of a second. This is accompanied with a smaller C parameter at the end of go period ($C_{max} = 3.89$ for $v = 40$ nm/s). It is also worth to note that the motion distance increases up to 50 nm and the sudden decrease occurs up to 15 nm corresponding to above-mentioned decrease of τ_{go} and τ_{stop}.

The same tendency is visible for the $v = 10$ nm/s and different values of the α lamella thickness (Table 2). The abrupt change of τ_{go} and τ_{stop} values takes place for the λ_α equal to 250 nm. Also, the C_{max} is in the same range as for the assumed $\lambda_\alpha = 100$ nm and v in the range of 10 and 40 nm/s. The only one difference is in the total distance covered by the RF which is much shorter for the $\lambda_\alpha = 250$ and 300 nm and equal to 6 and 4 nm (Table 2).

4 Discussion

The presented results clearly show the nature of go-and-stop motion. The process takes place in the successive stages which can be distinguished judging from the value of C parameter. However, the time necessary to accomplish the full cycle with relaxation (that means one go and one stop period) can completely be different. For lower values of

linear growth rate ($v = 10 \div 20$ nm/s) and smaller α lamella thickness ($100 \div 200$ nm), the full cycle with relaxation takes 4–6 s. The faster movement of the RF ($v = 30$ nm/s) resulted in a dramatic decrease of the full cycle to $\tau_{total} = 0.8$ s. The same behavior is observed if the α lamella thickness increases beyond 200 nm at constant v equal to 10 nm/s.

The obtained results can be compared with those of Abdou et al. [1] for the Al-15 at.% Zn alloy aged at 433 K. They reported that the distance between two elementary go-and-stop events (full cycle with relaxation) was 30–90 nm and the largest stop interval of 4 s. This is larger than 20–50 nm obtained in the present study but corresponds well with 2–3 s shown in Tables 1 and 2. However, this is in disagreement with the maximum growth rate 110 nm/s for time of 0.7 s measured by Abdou et al. [1]. On the other hand, the results shown in Table 1 indicate very short time of motion (τ_{go}) equal to 0.2 s but for the growth rate smaller by factor 3. Such a discrepancy can be explained if we reconsider once again Fig. 1 in Ref. [1]. Then, we can easily see that not each go period is characterized by a huge jump of the growth distance. There are also intervals for which the gain of the distance is much smaller and it obviously does not correspond to the stop period. Those smaller gains take less than 5 s. This means that we can expect two modes of the go-and-stop motion for which the growth takes either few seconds or tenths of second which confirms the results obtained in the present paper.

On the other hand, the energy-dispersive X-ray microanalysis (EDS) analysis made in the middle of α lamella revealed the changes of Zn content between 13 and 7 at.% for two successive stages of go-and-stop motion and for the distance of about 300 nm for the Al-22 at.% Zn alloy aged at 423 K [12]. If we take the typical linear growth rates for DP process from Ref. [16] and the same alloy aged at 428 K migration for such distance requires ca. $\tau_{go} = 7–21$ s. One should remember that the linear growth rate determined by Solorzano et al. [16] was averagely taken from 10

Table 1 Results of simulation for $\lambda_\alpha = 100$ nm and various values of v

Stage	Time (s)	Parameter C	Movement distance (nm)	Stage	Time (s)	Parameter C	Movement distance (nm)
$v = 10$ nm/s, $\lambda_\alpha = 100$ nm				$v = 30$ nm/s, $\lambda_\alpha = 100$ nm			
Go	1	2.47	10	Go	0.1	1.13	3
	2	6.37	20		0.2	1.62	6
	3	9.56	30		0.3	2.44	9
Stop	4	5.4	30		0.4	5.25	12
	5	3.77	30		0.5	6.56	15
	6	1.71	30	Stop	0.6	4.05	15
Go	7	2.47	40		0.7	2.4	15
	8	6.37	50		0.8	1.03	15
	9	9.56	60	Go	0.9	1.13	18
Stop	10	5.4	60		1	1.62	21
	11	3.77	60		1.1	2.44	24
	12	1.71	60		1.2	5.25	27
$v = 20$ nm/s, $\lambda_\alpha = 100$ nm					1.3	6.56	30
Go	1	2.66	20	Stop	1.4	4.05	30
	2	6.77	40		1.5	2.4	30
Stop	3	3.26	40		1.6	1.03	30
	4	1.37	40	$v = 35$ nm/s, $\lambda_\alpha = 100$ nm			
Go	5	2.66	50	Go	0.1	1.38	3,5
	6	6.77	60		0.2	2.22	7
Stop	7	3.26	60		0.3	5.63	10.5
	8	1.37	60	Stop	0.4	2.3	10.5
$v = 25$ nm/s, $\lambda_\alpha = 100$ nm					0.5	0.89	10.5
Go	1	2.7	25	Go	0.6	1.38	14
	2	6.9	50		0.7	2.22	17.5
Stop	3	3.91	50		0.8	5.63	20
	4	1.84	50	$v = 40$ nm/s, $\lambda_\alpha = 100$ nm			
Go	5	2.7	75	Go	0.1	1.94	4
	6	6.9	100		0.2	3.89	8
Stop	7	3.91	100	Stop	0.3	1.71	8
	8	1.84	100	Go	0.4	1.94	12
					0.5	3.89	16
				Stop	0.6	1.71	16

measurements of average cell width versus time. If we take in situ determined linear growth rate even at lower temperature of 400 K the resulting time is 2.5–5.3 s [9]. This is in a good agreement with the data presented in Table 2 for low v and λ_α.

The EDS technique was also used in a Co-13 at.% Al alloy for the determination of Al-concentration profiles across the α lamella at the various distances from the RF [11]. Three maxima of the parameter C around 5.2 ± 5.4 were distinguished. Then, abrupt change down to 3.4 ± 3.7 was observed. Such a sequence repeated three times over the distance of 350 nm. This means that go period was extremely short approaching $\tau_{go} = 1.12$ s for the linear growth rate 89 nm/s or even $\tau_{go} = 0.23$ s for 432 nm/s [11]. Again, we have a good fit with our results and indication that this second type of movement takes tenths of second. Further, if

we compare the values of C_{max} (Tables 1 and 2) we can see that in most cases these values are between 5.29 and 6.56 which is in good agreement with the results obtained for the Co-13 at.% Al alloy. The discrepancy concerning the lowest values of C preceding subsequent stage of movement can be attributed to the fact that the solute concentration profiles should be made with the step 1–4 nm which was not a case in the Co-13 at.% Al alloy [11].

The examination of the DD reaction at 885 K after DP at 723 K in Fe-13.5 at.% Zn alloy revealed "ghost images" of the successive positions of the receding RF with the distance between two neighboring "ghost lines" ca. 0.2-0.3 μm (see Figs. 4b, c in Ref. [7]). The average velocity of receding RF determined from measurements 50 "ghost images" width was 50 nm/s. In such a way, time for the go distance should be ca. $\tau_{go} = 4–6$ s. The same analysis made for the Cu-Cd

Table 2 Results of simulation for $v = 10$ nm/s and various values of λ_α

Stage	Time (s)	Parameter C	Movement distance (nm)	Stage	Time (s)	Parameter C	Movement distance (nm)
$v = 10$ nm/s, $\lambda_\alpha = 100$ nm				Stop	0.7	4.3	6
Go	1	2.47	10		0.8	3.11	6
	2	6.37	20		0.9	2.4	6
	3	9.56	30		1	1.67	6
Stop	4	5.4	30	Go	1.1	2.12	7
	5	3.77	30		1.2	3.3	8
	6	1.71	30		1.3	4.67	9
Go	7	2.47	40		1.4	5.35	10
	8	6.37	50		1.5	5.67	11
	9	9.56	60		1.6	5.84	12
Stop	10	5.4	60	Stop	1.7	4.3	12
	11	3.77	60		1.8	3.11	12
	12	1.71	60		1.9	2.4	12
$v = 10$ nm/s, $\lambda_\alpha = 200$ nm					2	1.67	12
Go	1	2.3	10	$v = 10$ nm/s, $\lambda_\alpha = 300$ nm			
	2	5.98	20	Go	0.1	2.03	1
Stop	3	2.91	20		0.2	3.17	2
	4	1.03	20		0.3	4.44	3
Go	5	2.3	30		0.4	5.29	4
	6	5.98	30	Stop	0.5	3.77	4
Stop	7	2.91	30		0.6	1.71	4
	8	1.03	30	Go	0.7	2.03	5
$v = 10$ nm/s $\lambda_\alpha = 250$ nm					0.8	3.17	6
Go	0.1	2.12	1		0.9	4.44	7
	0.2	3.3	2		1	5.29	8
	0.3	4.67	3	Stop	1.1	3.77	8
	0.4	5.35	4		1.2	1.71	8
	0.5	5.67	5				
	0.6	5.84	6				

alloys containing 1.82 and 2.75 wt% Cd after prior aging at 623 K and dissolved at 813 K (Figs. 5 and 6 in Ref. [4]) provided the average distance between two successive "ghost lines" ca. 1.0 and 1.25 μm, respectively. This can only be compared with the average velocities 88 and 417 nm/s determined by measurements receding distances of the RF versus time of dissolution [4]. The resulting time is between 11 and 3 s. Obviously, for all the above-discussed cases the real go time should be much shorter as the average DD velocity takes into account both go-and-stop periods. This could be even one order of magnitude as it was pointed out by Abdou et al. [1] for the DP in the Al-15 at.% Zn alloy.

The presented examples support the idea that two different modes of go-and-stop motion of the RF operate during DP. However, which mechanism is responsible for, remains unclear. We may only speculate that a specific crystallographic or solute concentration instability can lead to the small oscillations of the RF which result in small gain of the growth distance. Such small oscillations of order of

2 nm were predicted by Klinger et al. [17] who attributed the obtained results to non-steady state existing along the RF of discontinuous precipitates. On the other hand, better stability of the system should allow for longer time during which the RF can move.

5 Conclusions

The simple procedure involving Cahn's equation was presented to visualize the behavior of go-and-stop motion during DP process. The results of simulation revealed two types of such motion. The first one with longer time interval approaching several seconds is typical for rather small values of the linear growth rate of the RF and α phase lamella thickness. The second type which takes only tenths of second is attributed to much faster movement of the RF and relatively large thickness of the α phase lamella.

Both predicted types of go-and-stop motion can experimentally be observed during growth or dissolution of discontinuous precipitates. What is the reason that particular type prevails is unknown, and this is invitation for further studies especially using high-resolution transmission electron microscope operating in in situ mode.

References

1. Abdou S, Solorzano GI, El-Boragy M, Gust W, Predel B. In-situ study of discontinuous precipitation in Al-15 at.% Zn. Scripta Mater. 1997;34:1431–6.
2. Bögel A, Gust W. A standardized model and a reaction principle for discontinuous precipitation. Z Metallkd. 1998;79:296–308.
3. Chongmo L, Hillert M. A metallographic study of diffusion-induced grain boundary migration in the Fe–Zn system. Acta Metall. 1981;29:1949–60.
4. Sulonen MS. Discontinuous mode of dissolution of a β phase precipitate into α Cu–Cd solid solutions. Acta Metall. 1960;8:669–76.
5. Tu KN, Turnbull DB. Morphology and kinetics of cellular dissolution of the Pb-Sn alloy. Metall Trans A. 1971;2:2509–15.
6. Hackney SA, Biancaniello FS. Directional invariance of grain boundary migration in the Pb-Sn cellular transformation and the Tu-Turnbull hysteresis. Scripta Metall. 1986;20:1417–22.
7. Chuang TH, Fournelle RA, Gust W, Predel B. Drei diskontinuierliche Festkörperreaktionen in einer a-Fe-13.5 At.% Zn-Legierung. Z Metallkd. 1989;80:318–26.
8. Pawłowski A, Zięba P. Mechanism of early stages of discontinuous dissolution in AlZn alloys. Mater Sci Eng, A. 1989;108:9–17.
9. Zięba P, Gust W. Local values of the diffusivities at the migration front of the discontinuous precipitates in Al-22 at.% Zn alloy. Scripta Mater. 1998;39:13–20.
10. Zięba P, Gust W. Microanalytical study of discontinuous precipitation and dissolution in Ni-4 at.% Sn: local and global characterization of the reactions. Acta Mater. 1999;47:2641–50.
11. Zięba P. Microanalytical study of the discontinuous precipitation in a Co-13 at.% Al alloy. Acta Mater. 1998;46:369–77.
12. Chung YH, Shin MC, Yoon DY. In situ observation of discontinuous precipitation in an Al-40 wt% (21.8 at.%) Zn alloy. In: Kim NJ, editor. Proceedings of the international symposium on light materials for transportation systems (LiMAT-93). Center for Advanced Aerospace Materials, Pohang University of Science and Technology; 1993. p. 371–6.
13. Cahn JW. The kinetics of cellular segregation reactions. Acta Metall. 1959;7:18–28.
14. Tashiro K, Purdy GR. In situ observations of chemically induced grain boundary migration and discontinuous precipitation in the aluminum–zinc system. Metall Trans A. 1989;20:1593–600.
15. Zięba P. In situ study of discontinuous precipitation and dissolution in an Al-22 at% Zn alloy. Z Metallkd. 1999;90:669–74.
16. Solorzano IG, Purdy GR, Wheatherly GC. Studies of the initiation, growth and dissolution of the discontinuous precipitation product in aluminum-zinc alloys. Acta Metall. 1984;31:1709–17.
17. Klinger L, Brechet Y, Duly D. On the influence of non-steady state velocity on interlamellae concentration profiles in discontinuous precipitation. Scripta Mater. 1997;37:1237–42.

Publisher's Note Springer Nature remains neutral with regard to jurisdictional claims in published maps and institutional affiliations